Conference Paper, Published Version

Zeng, J.; Constantinescu, George; Weber, L.

Prediction of scoured bed and sediment transport at equilibrium conditions in curved alluvial channels using advanced near wall models

Prediction of scoured bed and sediment transport at equilibrium conditions in curved alluvial channels using advanced near wall models

J. Zeng, G. Constantinescu and L. Weber
Department of Civil & Environmental Engineering, IIHR-Hydroscience and Engineering,
The University of Iowa, Iowa City, IA 52242; USA

I. INTRODUCTION

Strongly curved alluvial river reaches and channels are especially affected by scour phenomena over time due to the presence of strong secondary motions in transverse sections. These secondary motions generate highly irregular bed profiles. As a consequence, the channel navigability and bank stability are strongly dependent on the evolution of the bed deformations in time. Additionally, sediment erosion and deposition in time can have important environmental repercussions for the river. Presence of hydraulic structures in regions of strong flow curvature tends to amplify local scour phenomena around these structures. Thus, prediction of the bathymetry and scour at equilibrium conditions is of great interest for river engineering applications.

Before considering complex applications involving river reaches of complex bathymetry, it is important to focus on simpler problems that retain most of the complexity of real applications, but allow to separate the effects of some of the main factors contributing to the bed evolution in real applications. In this paper we consider only curved channel bends of rectangular section with non-erodible banks in which a uniform thick layer of sand is originally present on the bottom of the channel.

In the region of strong channel curvature, due to the action of the centrifugal forces, the fluid particles follow a helical motion. As a consequence of the action of these forces, a pressure gradient is induced between the two banks in the region of high curvature such that the fluid and sediment particles move from the outer bank toward the inner bank in the near bed region. The main characteristic of the bed scouring in these bends is the formation of a point sand bar near the inner bank and of a pool at the outer part of the bend. The transversal distribution of the streamwise velocity is also affected by this strong secondary flow which induces a vertical velocity component in the transversal section and locally modifies the magnitude and direction of the bed shear stress. In the outer regions, where the bed shear stress is strongly amplified, local scour phenomena develop in time. The transversal slope increases until the force induced by the secondary current against the transversal slope is balanced by the (downwards) component of the gravitational force acting on the sediment particles in the same direction. At this point the flow and sediment transport are at equilibrium.

In the present paper, we try to predict the equilibrium flow, sediment transport and bathymetry using a fully three-dimensional (3D) Reynolds-Averaged Navier-Stokes (RANS) non-hydrostatic numerical model using advanced turbulence models ([1], [2]). The use of such a sophisticated model is needed because of the strong transverse non-uniformity of the flow in regions of high channel curvature and of the non-local nature of the sediment entrainment / deposition processes. The model is fully coupled. The bed changes induced by deposition / erosion phenomena affect the flow which, in turn, influences not only the advection of the suspended sediment but also the distribution of the bed shear stress. Thus, the distribution of the bed load component will also change.

II. BACKGROUND ON NUMERICAL MODELING OF FLOW AND SEDIMENT TRANSPORT IN ALLUVIAL CHANNELS

Due to their obvious limitations, 1D models are clearly not appropriate to predict bathymetry changes in curved alluvial channels in which large variations of the bed profiles are present in the transverse direction. Two-dimensional (2D) model are much more successful and are presently the most common approach used to predict flow and sediment transport in curved bends with movable beds. Duc et al. [3] gives a good description of some of the most popular of these 2D models based on finite differences, finite volume or the finite element approach ([4], [5]). Because of the information lost through the depth-averaging process, these 2D models are limited, to a degree or another, by the fact that they cannot account correctly for the effects of strong secondary currents on the flow and sediment transport, or for non-equilibrium effects. The usual way to account for some of these three-dimensional effects in 2D depth-averaged models is to introduce empirical secondary flow corrections. However, these corrections typically assume fully developed flow in the bend, require additional assumptions about the radius of curvature of the flow streamlines and do not account for the coupling between the primary and secondary flows. Thus, these models are in fact limited to flows with moderate streamline curvatures. Even in these cases, to obtain accurate results using these models lots of calibration of the empirical model constants is needed.

A more complex variant of these 2D models that tries to incorporate more of the original 3D characteristics of the

secondary flow into the depth-averaged model ([6], [7]) uses additional conservation equations for the moment of the momentum equations. These quasi-3D models can account in a physically more correct way for the redistribution of the bed shear stress magnitude caused by the momentum transfer between the streamwise and the transversal flows along the channel. Another quasi-3D model was proposed by van Rijn [8]. In his model the sediment transport was calculated in 3D while the horizontal mean flow was obtained using a 2D depth-averaged model. The vertical velocity profile needed in the sediment transport module was assumed to be logarithmic.

The next level of modeling is the use of fully 3D hydrostatic models. Gessler et al. [9] integrated a complex mobile-bed module into a 3D hydrostatic code CH3D that uses the σ-stretching technique in the vertical direction. Their mobile-bed module developed for sand-rivers included several processes such as aggradation and scour, bed-material sorting, and accounted for the movement of non-uniform sediment mixtures as bed load and suspended load. Though clearly incorporating more physics than 2D depth averaged models, the accuracy of the flow and sediment predictions using 3D hydrostatic models in strongly curved river reaches or channels, where strong secondary motions are present and separation may occur, is also limited.

One of the first successful applications of a fully 3D non-hydrostatic finite-volume model for movable bed applications was reported by Olsen [10]. The model successfully predicted the formation of the meandering pattern in an initially straight alluvial channel and accounted for wetting and drying caused by channel erosion / deposition. Both the suspended load and the bed load were simulated. The k-ε model with wall functions was used. The same code was used in [11] to predict flow and sediment transport in a narrow 90^0 curved bend. Another 3D non-hydrostatic finite-volume model that was used to calculate the equilibrium flow, sediment transport and bathymetry in curved channel bends was proposed by Wu et al. [12]. Their modeling of the bed load was more sophisticated and was based on the non-equilibrium method proposed in [8]. The water surface deformation was calculated from a 2D Poisson equation for the surface height obtained from the depth-averaged 2D momentum equations. The k-ε model with wall functions and corrections for rough surfaces was used. The model was subsequently used in [13] to predict the flow and suspended sediment transport for the reservoir generated by the dam of the Three Gorges Project on the Yangtze River.

Because of the empiricism related especially to the bed load transport modeling, model validation and a certain degree of calibration (though much more reduced than the one required by 2D depth-averaged or quasi-3D models) is necessary even in fully 3D models. Thus, comparison of computed results with experimental data corresponding to well-controlled laboratory experiments is essential before application of the model to predict equilibrium flow, sediment and scoured bed geometry in realistic river reaches.

III. FLOW SOLVER

The incompressible RANS and turbulence transport equations are first transformed in generalized curvilinear coordinates. However, the primitive variables (Cartesian velocity components, V_i) for which the momentum equations are solved are left unchanged (partial transformation approach). The continuity and momentum equations are:

$$J\frac{\partial}{\partial \xi^j}\left(\frac{V^j}{J}\right) = 0 \tag{1}$$

$$\frac{\partial Q}{\partial t} + A_j\frac{\partial Q}{\partial \xi^j} - J\frac{\partial E_{vj}}{\partial \xi^j} + H_p = 0 \tag{2}$$

where x_i are the Cartesian coordinates and ξ^j are the curvilinear coordinates. In equation (2), $Q=(V_1,V_2,V_3)^T$ is the Cartesian velocity vector; J is the Jacobian $J=\partial(\xi^1,\xi^2,\xi^3,)/\partial(x_1,x_2,x_3)$, $V^i = V_j\xi^j_{x_i}$ are the contravariant velocity components, A_j= diag(V^1, V^2, V^3) and $E_{vj} = (E^1_{vj}, E^2_{vj}, E^3_{vj})$ are the vectors containing the viscous and turbulence fluxes and, finally, H_p is the pressure gradient vector

$$H_p = \left(\xi^k_{x1}\frac{\partial \psi}{\partial \xi^k}, \xi^k_{x2}\frac{\partial \psi}{\partial \xi^k}, \xi^k_{x3}\frac{\partial \psi}{\partial \xi^k}\right)^T . \tag{3}$$

The governing equations are non-dimensionalized using a length scale H_0 (water depth at the inlet) and a velocity scale U (bulk velocity in the inlet section) such that formally the Reynolds number ($Re=UH_0/\nu$) replaces the molecular viscosity ν, and the Froude number ($Fr=U/(gH_0)^{0.5}$) is used to scale the free surface deformations. The modified pressure χ is defined as $\chi=p+2/3k$ and the effective piezometric pressure P is defined as $P=p/\rho+z/Fr^2-2/3k$, where p is the pressure, z is the free surface elevation and k is turbulence kinetic energy. The Froude number enters the solution through the free-surface boundary condition assuming that the deformable free surface model is turned on (for more details on the free surface module see [1]). The velocity components are set equal to zero on all solid surfaces. At the outflow all variables are extrapolated from the interior. The pressure is extrapolated from the interior of the domain on all boundaries except at the free surface.

The eddy viscosity in the simulations discussed in the present paper is provided by the k-ω (SST) model. As the standard form of the k-ω (SST) model was used, only the implementation of the boundary conditions is discussed. The turbulence kinetic energy k is set equal to zero at the walls. For smooth surfaces, ω is calculated as $\omega = 800\nu/(\Delta n_1^2)$ where Δn_1 is the normal distance to the wall of the first grid point off the wall. For rough

surfaces, $\omega = 2500\nu/(k_s)^2$ for $k_s^+ < 25$ and $\omega = 100u_*/k_s$ for $25 < k_s^+$, where k_s is equivalent roughness height ($k_s^+ = u_* k_s/\nu$) and u_* is the friction velocity.

The equivalent bed roughness is estimated using a formula proposed by van Rijn [8] in the case in which small bed forms are present:

$$k_s = 3d_{90} + 1.1\Delta(1 - e^{-25\psi}) \tag{4}$$

where the first term accounts for the sand grain roughness contribution and the second term represents the bed form contribution. In equation (4), $\psi = \Delta/\lambda$ where Δ and λ are the height and length of the sand waves, respectively. Following Wu et al. [12], the length λ is assumed to be $\lambda = 7.3H$ and the parameter ψ is estimated from:

$$\psi = \Delta/\lambda = 0.015(d_{50}/H)^{0.3}\left(1 - e^{-0.5T}\right)(25 - T) \tag{5}$$

in which H is the local water depth, d_{50} and d_{90} are the median and 90% diameters of the bed material, and T is the non-dimensional excess shear stress. Its expression is given in [8] and [1].

A fractional step method is used to solve the RANS equations. All terms in the pressure Poisson equation are discretized using second-order accurate central differences. The momentum and turbulence transport equations are discretized using second order accurate upwind differences for the convective terms. All other operators are calculated using second-order central discretizations. All terms are treated implicitly, including the source terms in the transport equations for turbulence quantities. To accelerate the convergence of the resulting system of equations toward steady state (equilibrium), local time-stepping techniques are used. An approximate factorization technique is used to simplify the inversion of the discrete form (left hand side) of the momentum, pressure-Poisson and turbulence transport equations. The equations are solved implicitly using the alternate-direction-implicit (ADI) method. The implementation of the deformable free surface module in which the proper kinematic and dynamic boundary conditions are applied at the top boundary is described in [1].

IV. SEDIMENT TRANSPORT AND MOVABLE BED MODELS

An advection-diffusion scalar transport equation with an additional settling-velocity source term is solved to determine the local sediment concentration C and the suspended sediment fluxes at the top of the bed load layer for simulations in which the suspended sediment load cannot be neglected. The equation is not solved up to the wall, as are the momentum equations, but rather up to the interface with the bed load layer (δ(x,y)) which typically corresponds to a k=constant surface in the computational domain. In curvilinear coordinated, the equation is:

$$\frac{\partial C}{\partial t} + V^j \frac{\partial C}{\partial \xi^j} - \omega_s \delta_{3i} \frac{\partial C}{\partial \xi^j}\frac{\partial \xi^j}{\partial x_i} - J\frac{\partial}{\partial \xi^j}\left(\frac{g^{ij}}{J}\left(\frac{\nu + \nu_t}{\sigma_c}\right)\frac{\partial C}{\partial \xi^i}\right) = 0 \tag{6}$$

where ω_s is the setting velocity of the sediment, δ_{3j} is the Kronecker delta symbol with $j=3$ indicating the vertical direction and σ_c is the Schmidt number. Its role is to relate the sediment (turbulent) diffusivity to its (eddy) viscosity. At the free surface, the total vertical flux of suspended sediment is set to zero:

$$\left(\frac{\nu + \nu_t}{\sigma_c}\right)\frac{\partial C}{\partial \xi^j}\frac{\partial \xi^j}{\partial x_3} + \omega_s C = 0 \tag{7}$$

At the interface between the suspended sediment and the bed load layers situated not far, but not necessarily at the reference level $z=a$, following van Rijn [8] and Wu et al. [14], the entrainment rate is assumed to be equal to the one under equilibrium conditions. The total vertical sediment flux at the interface is equal to the net sediment transport (deposition minus entrainment) across the interface. This can be written as

$$\left(\frac{\nu + \nu_t}{\sigma_c}\right)\frac{\partial C}{\partial \xi^j}\frac{\partial \xi^j}{\partial x_3} + \omega_s C = D_b - E_b = \omega_s C - \omega_s C_{b**} \tag{8}$$

where C_{b**} is the equilibrium concentration at z=δ, $D_b = \omega_s C_b$ is the deposition rate and $E_b = \omega_s C_{b**}$ is the entrainment rate at the top of the bed layer. The value of C_{b**} can be calculated assuming Rouse formula to be valid between the reference level where $C = C_{b*}$ ($z=a$) and the interface between the bed and the suspended load layers (z=δ(x,y)). There is no unique way to choose the reference level a. In some cases it is taken equal to the bed roughness, in other cases it is taken as a percentage of the total depth. At the inlet section a concentration profile needs to be prescribed, while at the sidewalls and outlet a zero gradient boundary condition is imposed.

The empirical formulas proposed in [8] are used to estimate the equilibrium concentration at the reference level (C_{b*}) needed to calculate C_{b**} in (8), the equilibrium bed load transport rate (Q_{b*}) and the non-equilibrium adaptation length (L_s). Their detailed expressions are also given in [1] and [2] along with several methods to numerically estimate the local bed shear stress τ_*. The

equilibrium bed load transport rate and the non-equilibrium adaptation length are needed to close the non-equilibrium bed transport model (see (10) below). Following [12], the mass balance equation for the sediment within the bed load layer, in which the storage term is neglected, is:

$$(1-p')\frac{\partial z_b}{\partial t} - D_b + E_b = -\nabla Q_b = \\ -J_b\left(\frac{\partial}{\partial \xi}\left(\frac{Q_{b\xi}}{J_b}\right) - \frac{\partial}{\partial \eta}\left(\frac{Q_{b\eta}}{J_b}\right)\right) = 0 \quad (9)$$

In the above equation p' is the porosity, J_b is the Jacobian of the geometric transformation in the bed load layer, $(J_b = \partial(\xi, \eta)/\partial(x, y))$, z_b is the bed level above a datum, $Q_{b\xi}$ and $Q_{b\eta}$ are the components of the bed-load transport in the two directions. Then, in the present model we use the same non-equilibrium bed-load model as in [12] in which the relation between the bed change due to deposition from the bed load layer and the bed load transport rate is:

$$(1-p')\frac{\partial z_{b\_bed\_load}}{\partial t} = \frac{1}{L_s}(Q_b - Q_{b*}) \quad (10)$$

such that the total change in the bed elevation is:

$$(1-p')\frac{\partial z_b}{\partial t} = D_b - E_b + \frac{Q_b - Q_{b*}}{L_s}. \quad (11)$$

The equation for the bed load rate Q_b is derived from (9) in which we made the substitution corresponding to the model assumed in (11):

$$\frac{(Q_b - Q_{b*})}{L_s} + \nabla Q_b = 0 \quad (12)$$

Equation (12) which is solved to determine the bed load Q_b is the same for the case when the suspended sediment transport module is active and for the case when the suspended sediment transport can be neglected.

To close the model, one has to express $Q_{b\xi}$ and $Q_{b\eta}$ in (9) and (12) as a function of Q_b. When the bed becomes sloped, the gravitational force on the particles will resist the shear force to further carry the particles to the upper part of the slope. The sediment transport direction will deviate from the local direction of the bed shear stress. Especially for simulations in which the suspended sediment load becomes comparable or larger than the bed load, it is important to account for bed slope effects on the total load Q_T and not only on the bed load component, as it is generally done. To do that, in our model we define the total load (considered as a vectorial relationship in the horizontal directions) as simply:

$$Q_T = Q_b + Q_S \quad (13)$$

where Q_S is the suspended sediment load flux in the local water column from the top of the bed layer to the free surface. By taking the divergence of (13) we obtain, using the mass conservation equation in the water column corresponding to the suspended sediment domain (between z=δ(x,y) and free surface) and neglecting the storage term,

$$\nabla Q_T = \nabla Q_b + \nabla Q_S = \nabla Q_b - D_b + E_b. \quad (14)$$

Then, we rewrite (12) for the total load using (13) and (14) as

$$\frac{1}{L_s}(Q_T - Q_S - Q_{b*}) + \nabla Q_T + D_b - E_b = 0. \quad (15)$$

As the new variable in (15) is Q_T, we rewrite (11) as

$$(1-p')\frac{\partial z_b}{\partial t} = -\nabla Q_T \quad (16)$$

where use was made of (9) and (14). At this point the model is closed, provided that we are able to estimate Q_S from the concentration field and a formula to split Q_T after the two horizontal directions (ξ, η) is available.

To evaluate Q_S, one simply has to apply the definition to calculate the two components of the flux of suspended sediment in the two horizontal directions (x,y) as

$$Q_{Sx} = \int_{\delta}^{h}\left(uC - \frac{\nu + \nu_t}{\sigma_c}\frac{\partial C}{\partial x}\right)dz' \quad (17)$$

$$Q_{Sy} = \int_{\delta}^{h}\left(vC - \frac{\nu + \nu_t}{\sigma_c}\frac{\partial C}{\partial y}\right)dz'. \quad (18)$$

The magnitude of the suspended sediment flux is:

$$Q_S = \sqrt{\left(Q_{Sx}^2 + Q_{Sy}^2\right)}. \quad (19)$$

To introduce bed slope effects directly for Q_T, the formula proposed by Sekine and Parker [14] for bed slope effects affecting the bed load transport is used, but with Q_b replaced by Q_T:

$$Q_{T\eta} / Q_{T\xi} = \left(\sin\theta_b - \beta \frac{\partial z_b}{\partial l_\eta} \right) / \left(\cos\theta_b - \beta \frac{\partial z_b}{\partial l_\xi} \right) \qquad (20)$$

where $\theta_b = \tan^{-1}(\tau_{*\eta} / \tau_{*\xi})$ is the angle between the bed shear stress vector and the streamwise direction, $\beta = \beta^*(\tau_c^*/\tau_L^*)^m$, τ_L^* is the nondimensional longitudinal Shield stress $\tau_L^* = \tau_* \cos\theta_b / \rho R g d_{50}$, $R = \rho_s/\rho - 1$, ρ_s is the sediment density, ρ is the water density, the critical shear stress $\tau_c^* = \rho u_{*cr}^2$ is given by Shields diagram, m is a coefficient (m=1), $\beta^* = \alpha_G / \tau_c^*$, $\partial z_b/\partial l_\xi$, $\partial z_b/\partial l_\eta$ are the streamwise and transverse bed slopes, and α_G is a coefficient typically in the range 0.45-0.7. In the present simulations we used α_G=0.6.

Thus, the divergence operator ∇Q_T can be calculated in curvilinear coordinates (ξ,η). Once z_b is calculated from (16), the grid points between the bed level and the free surface are redistributed vertically based on the new positions of the water surface and bed level elevations.

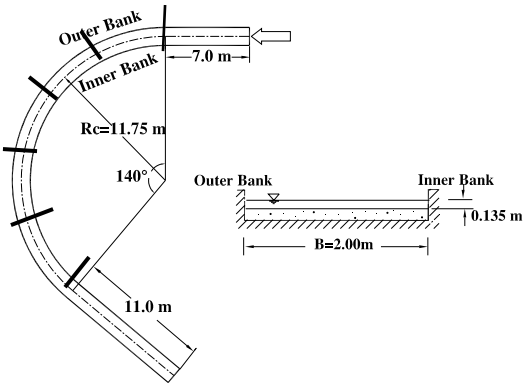

Figure 1. Flume layout and cross section geometry at the start of the 140^0 curved bend experiment of Olesen [15].

V. RESULTS

The equilibrium flow, sediment transport and scoured bed in the 140^0 curved bend of rectangular section (see sketch in Figure 1) studied experimentally by Olesen [15] are computed in the present study. Specifically, we validate our method by computing the flow corresponding to the experimental conditions in test case T4 in [15]. The curvature radius of the flume in the curved region was 11.75m. Both ends of the curved region (bend) were connected to straight channels toward the inflow and outflow sections. Their lengths were 7m and 11m, respectively. The width of the channel was B=2.0m wide. The inflow discharge was $0.118 m^3/s$. The mean inlet velocity was U=0.44 m/s and the water depth at the inlet was H_0=0.135m. The Froude and Reynolds numbers upstream of the curved region were 0.38 and 59,400, respectively. The incoming flow was fully turbulent. The flume bed in the experiment was initially leveled with a layer of relatively uniform sand whose thickness was 0.3m. The mean sand diameter was d_{50}=0.80mm (d_{90}=1.61mm). The main parameters of the experiment are summarized in Table 1. The experiment was run for approximately 72 hours to reach equilibrium steady state. In the experiment it was observed that the sediment moved mainly as bed load. The bathymetry and water levels were then measured at several selected sections. These measurements are used for validation of the present numerical model.

The flow was simulated on a computational mesh with close to 350,000 grid points (99x101x35 mesh points in the streamwise, spanwise and vertical directions, respectively). Two simulations were performed using the k-ω (SST) model. In the first simulation the contributions of both the bed load and the suspended sediment transport were considered (kω_total_load). In the second simulation only the bed load transport was considered, and the suspended sediment module was turned off. One of the goals of the present study is to investigate if the predictions of the equilibrium scour bathymetry are closer to experiment when considering both modes of sediment transport for a test case in which the suspended sediment transport is not thought to be important.

In both simulations the bottom roughness was estimated by using (4) and (5) in the initial straight part of the channel. The value of the bottom roughness k_S was found to be close to 0.0185m (~$20d_{90}$), corresponding to $k_S^+ \sim 920$ (well into the fully rough regime). The mean nondimensional value of the friction velocity at the bed was close to 0.11 in the same initial region. The side walls were considered smooth. The first points off the side-walls and channel bottom were situated at $\Delta n/H_0 \sim 0.0002$ ($\Delta n^+ \sim 0.7$).

Fully developed turbulent flow was specified at the inflow section. The profiles of the streamwise velocity and turbulent quantities were obtained from a preliminary simulation of the flow at the same Reynolds number in a straight periodic channel of identical section to that of the curved channel at its inlet section. Non-gradient conditions were used at the outlet to impose the velocity, concentration profile above the bed load layer and the value of the bed load transport rate.

The experimentally measured value of the bed-load transport rate (Q_b=0.0205 Kg/(ms)) was used to specify the inlet boundary condition for bed load transport. The suspended sediment concentration at the inlet was set equal to zero over the whole section as no measurements were available and the incoming flow is assumed to contain very little sediment above the bed load layer. The Schmidt number was equal to 0.85. The reference level corresponding to the thickness of the bed load layer (a) was assumed to be close to $3d_{90}$. This made that 16 mesh points were contained in the vertical direction inside this

TABLE 1. THE MAIN PARAMETERS OF THE EXPERIMENT CONDUCTED BY OLESEN [15]

Test Case	B (m)	H_0 (m)	U (m/s)	C (Chezy) ($m^{0.5}/s$)	I (surface slope)	d_{50} (mm)	d_{90} (mm)	Fr	Re
T4	2.0	0.135	0.44	29.9	$1.58x10^{-3}$	0.80	0.855	0.38	59,400

layer. This is different from models employing wall functions in which the bed load transport is generally assumed to occur within the first layer off the wall.

Similarly to the experiment, the simulations started from an initial flat bed and continued until equilibrium flow and bathymetry were reached in the curved channel. However, as we are using a steady state model in which local time stepping techniques are used to accelerate the convergence of the solution toward steady state, the transient in our numerical simulation is not expected to follow the evolution of the flow and bathymetry in the experiment. Only the steady state solution is expected to be close to the flow and bathymetry observed at equilibrium conditions in the experiment.

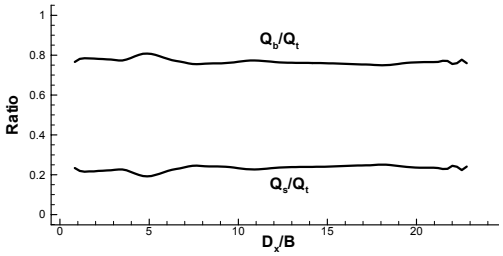

Figure 2. Predicted ratios of suspended sediment load and bed load to the total load along longitudinal direction in the kω_bed_load simulation.

Figure 2 shows the variation of the ratio of the cross-section averaged suspended sediment load to the total load (Q_s/Q_t) in the longitudinal direction for the kω_total_load simulation. The average value of this ratio for the simulated flow conditions is close to 0.2 over the whole length of the curved bend, confirming the fact that the suspended sediment component does not play an essential role in the overall sediment transport process.

The streamwise variation of the relative water depth at three positions situated 0.15B from the two banks and along the center line of the channel is shown in Figure 3. The longitudinal distance D_x, nondimensionalized by the width B of the channel, is measured along the centerline from the entrance in the straight reach of the channel. The entrance into the curved bend is situated at D_x=3.5B and the entrance into the downstream straight reach is situated around 18B. As no significant differences were observed in the distributions predicted by the two simulations, only the kω_total_load simulation results are shown. Overall, the predictions of the longitudinal water depth levels within the bend are in good agreement with measurements. In particular, the predictions near both banks are very close to the experiments in the region around the bend end ($15<D_x/B<20$). At the location situated 0.15B from the outer bank, the deepest scour is observed to occur in the experiment at $D_x/B\sim7$. The water depth at that location is $1.7H_0$. In the simulation the maximum scour occurs slightly downstream at $D_x/B\sim7.6$ and the water depth is somewhat underpredicted ($1.55H_0$). At the inner bank side, where a deposition sand bar has formed, the minimum water depth is observed to occur at $D_x/B\sim8.2$ in both simulation

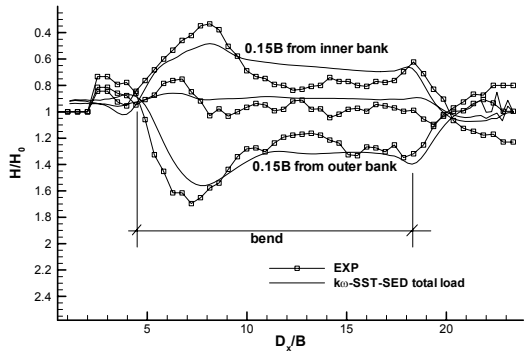

Figure 3. Comparison of longitudinal relative water depths at three positions inside the channel bend. H is local water depth. Only the results of simulation kω_bed_load are shown.

and experiment. However, at that location the flow is shallower in the experiment ($H=0.45H_0$) compared to simulation ($H=0.5H_0$). A second region, where some disagreement is observed between the simulation and experiment, is situated between D_x=10B and D_x=15B. Over this region the scour at the outer bank and the deposition at the inner bank are larger in experiment compared to simulation by about $0.1H_0$.

The numerical predictions of the water depth levels are compared with the measurements in Figure 4 at 12 cross-sections along the channel. The cross-sections cover the entire curved region of the channel, starting at its entrance (D_x/B=3.5), and the first 3.5B of the downstream straight reach (Figure 1). The transverse (lateral) slope gradually increases from zero at the bend entrance, to a maximum value that occurs at streamwise locations at which $9<D_x/B<10$. This region corresponds to the location of the highest sand bar and deepest scour hole (maximum water depth variation in the section is approximately 20cm in the experiment). The slope then slowly decays until $D_x/B\sim15$ and then remains almost constant until the end of the bend region (D_x/B=18.5). Once the flow enters the downstream straight reach, the

lateral slope returns quickly to horizontal and then becomes slightly negative. For example, in the section somewhat underpredicted in the simulations. For example, the maximum scour depth at the outer bank is

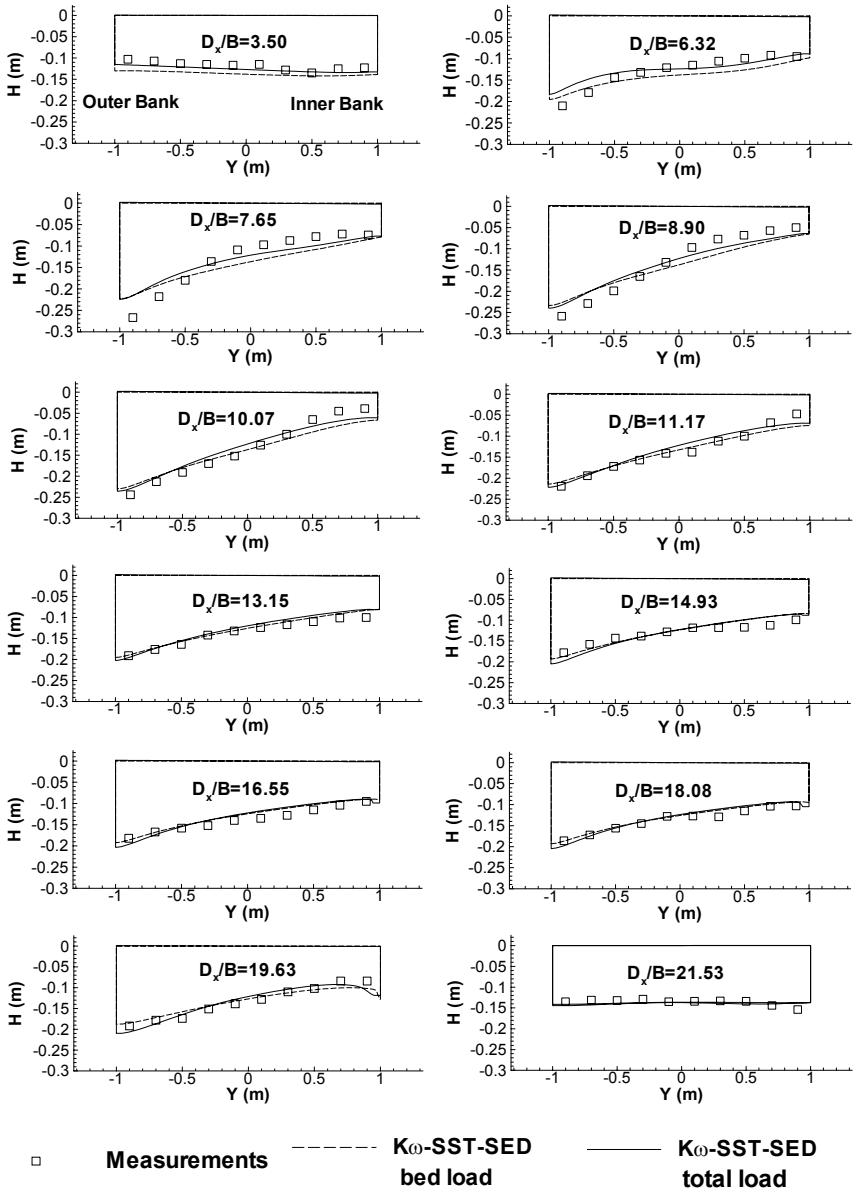

Figure 4. Comparison between predicted (kω_total_load and kω_bed_load simulations) and measured water depth levels at equilibrium conditions at different cross sections along the curved bend.

situated at $D_x/B=21.53$ the water depth is slightly higher near the inner bank, as the scour and deposition patterns switch to the opposite bank.

The variations of the water depth profile in the transversal direction predicted by the two simulations are found to be in good agreement with the ones obtained from experiment over the whole bend. The only region where some noticeable disagreement is observed is situated between $D_x/B=6$ and $D_x/B=11$. Over this region the largest differences in elevation between the two banks are observed in experiment. Though this is also true for the simulations, the maximum difference between the water depths in the regions close to the two banks is underpredicted by 1.5cm at $D_x/B=6.32$, by 4cm at $D_x/B=7.65$ and by 2.5cm in the section at $D_x/B=8.9$. Though the prediction of the maximum scour depth is very close to the experimental value at $D_x/B=10.07$, the water depth starts being overpredicted at the inner bank, where the level of the sand bar is about 1.5cm lower compared to the experiment.

As expected, the inclusion of the suspended sediment transport in the model did not have a large effect on the final equilibrium bathymetry. Still, the water depths predicted by the kω_total_load simulation appear to be slightly closer to the experiment in the middle of the channel ($-0.3m<Y<0.7m$) in the sections situated at

$D_x/B=7.65$ and $D_x/B=8.9$ where both simulations underpredicted the overall bed slope in the transversal section. The kw_bed_load simulation appears to overpredict by about 1cm the water depth at the entrance in the bend ($D_x/B=3.5$) over the whole section compared to experiment and to the kω_total_load simulation results.

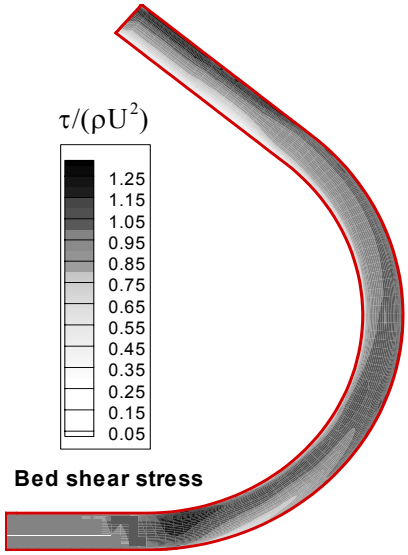

Figure 5. Distribution of the non-dimensional bed shear stress ($\tau/\rho U^2$) at equilibrium conditions in the kω_total_load simulation.

Figure 5 shows the contours of the predicted bottom shear stress ($\tau/\rho U^2$) inside the channel bend at equilibrium for the kω_total_load simulation. This distribution can not be obtained in an easy and accurate way from experiment. The distribution for the case in which only the bed load transport is considered was found to be quite similar and is not shown. The values of the bed shear stress in Fig. 4 are non-dimensionalized by the mean value of the bed shear stress at the inlet section obtained from the periodic straight channel simulation. As expected, a patch of relatively high bed shear stress values is present at the entrance into the bend closer to the inner wall. This happens because the position of the maximum streamwise velocity in sections close to the entrance into the curved region is situated closer to the inner wall. In fact, this effect, observed around the upstream part of the curved channel region in our simulation at equilibrium conditions, is present even for flat bed channels and was explained, among others, by Henderson [16] using Euler equations. As one moves downstream, the area of high bed shear stress gradually switches toward the deeper outer wall region inside the bend region.

For polar angles larger than 100^0 inside the bend, the maximum bed shear stress is observed to occur close to the outer bank. Interestingly, the maximum value in cross sections situated past the end of the curved region continues to increase for some distance in the downstream straight reach due to the transverse momentum acquired by the flow inside the bend. As one moves further downstream, the position of the maximum bed shear stress starts moving again toward the center of the section. Sane is true for the depth averaged streamwise velocity distribution (not shown). However, as observed from Fig. 4 this process is very slow and the distance needed for the distributions of the (depth-averaged) streamwise velocity and bed shear stress to recover the symmetrical shapes corresponding to fully developed flow in a straight channel is estimated to be of the order of 15-20B.

VI. SUMMARY

A fully 3D non-hydrostatic model developed by Zeng et al. [1,2] to predict the flow, free surface deformation, bed load, suspended sediment transport and bed morphology in open channels at equilibrium conditions was tested for the case of the flow in an 140^0 curved bend studied experimentally by Olesen [15]. One of the novelties of the present model is the use of RANS closures in versions that do not necessitate the use of wall functions and in which the small-scale bed roughness effects are incorporated via the specification of the wall boundary conditions.

The simulations confirmed the experimental observations that showed that most of the sediment moves as bed load. The suspended sediment load was estimated to contribute only 20% to the total sediment load for the flow and geometrical conditions considered in the test case. Consequently, the inclusion of the suspended sediment module in the numerical model did not affect significantly the equilibrium flow and bathymetry predictions. Comparison of the simulation results with the experimental data showed that the model was able to predict reasonably well the water depth levels over the whole length of the channel. A slight underprediction of the mean transverse bed slope was observed in the upstream part of the bend around the region where maximum scour occurs. The reason was an underprediction of the maximum scour depth at the outer bank, or an overprediction of the minimum water depth at the inner bank.

The model is being applied to predict flows in curved open channels with substantial amounts of suspended sediment transport and with very strong curvature in which three-dimensional effects are expected to be even more important than the ones present in the application considered in the present paper. Eventually, the goal will be to use the present model to predict equilibrium bathymetry in straight and curved channels containing hydraulic structures (e.g., bridge piers, bridge abutments, spur dikes, intakes, etc.) where local scour phenomena are important.

ACKNOWLEDGMENT

The authors would like to thank Professor A. Jacob Odgaard from IIHR-Hydroscience and Engineering, The University of Iowa for his insightful advice related to different aspects of this study.

REFERENCES

[1] Zeng, J., Constantinescu, G. & Weber, L.J. 2005a, A fully 3D non-hydrostatic model for prediction of flow, sediment transport and bed morphology in open channels, XXXIst International Association Hydraulic Research Congress, Seoul, Korea.

[2] Zeng, J., Constantinescu, S.G. and Weber, L.J. 2005b. Validation of a computational model to predict suspended and bed load sediment transport and equilibrium bed morphology in open channels. River and Coastal Estuarine Morphology Conference, The University of Illinois, Urbana Champaign, Illinois.

[3] Duc, B.M., Wenka, T and Rodi, W. 2004, Numerical modeling of bed deformation in laboratory channels, *J. Hydraulic Engineering*, 130(9), 894-904.

[4] Ghamry, H.K. and Steffler, P.M. 2005, 2D depth-averaged modeling of flow in curved open channels. *J. Hydraulic Research*, IAHR, 43(1), 44-55.

[5] Choi, S.U., Kim, T.B. and Min, K.D. 2005, 2D finite element modeling of bed elevation change in a curved channel, River and Coastal Estuarine Morphology Conference, The University of Illinois, Urbana Champaign, Illinois.

[6] Kassem, A.A. and Chaudhry, M.H. 2002, Numerical modeling of bed evolution in channel bends. *J. Hydraulic Engineering*, ASCE, 128(5), 507-514.

[7] Vasquez, J.A., Millar, R.G. and Steffler, P.M. 2005, Vertically-averaged and momentum model for alluvial bend morphology, River and Coastal Estuarine Morphology Conference, The University of Illinois, Urbana Champaign, Illinois.

[8] van Rijn, L.C. 1987, Mathematical modeling of morphological processes in the case of suspended sediment transport, *Delft Hydraulics Communication* No. 382, The Netherlands.

[9] Gessler, D, Hall, B., Spasojevic, M., Holly, F., Pourtaheri, H, Raphelt, N. 1999, Application of a 3D mobile bed, hydrodynamic model, *J. Hydraulic Engineering*, ASCE, 125(3), 737-749.

[10] Olsen, N.R. 2003, 3D CFD modeling of self-forming meandering channel, *J. Hydraulic Engineering*, 129(5), 366-372.

[11] Ruther, N. and Olsen, N.R. 2005, 3D modeling of sediment transport in a narrow 90^0 channel bend, *J. Hydraulic Engineering*, 131(10), 917-920.

[12] Wu, W., Rodi, W. and Wenka, T. 2000, 3D numerical modeling of flow and sediment transport in open channels, *J. Hydraulic Engineering*, 126(1), 4-15.

[13] Fang, H. and Rodi, W. 2003, 3D calculations of flow and suspended sediment transport in the neighborhood of the dam for the Three Gorges Project Reservoir in the Yangtze River, *J. Hydraulic Research*, 41(4), 379-394.

[14] Sekine, M. and Parker, G. 1992, Bed load transport on transverse slope, *J. Hydraulic Engineering*, 118(4), 513-535.

[15] Olesen, K.W. 1985, Experiments with graded sediment in the DHL curved flume, Report R 657 – XXII M 1771, Delft Hydraulics Laboratory.

[16] Henderson, F.M. 1966, Open Channel Flow. The Macmillan Company, New York.